Research Article

Comparing optical sensors spectral resolution using spectral libraries

Germain Forestier † * , Jordi Inglada ‡, Cédric Wemmert †† and Pierre Gançarski ††

† University of Haute Alsace, MIPS, Mulhouse, France
‡ CESBIO (CNES/CNRS/UPS/IRD), Toulouse, France
†† University of Strasbourg, LSIIT-CNRS UMR7005, Strasbourg, France

(*November 2011*)

In remote sensing data classification, the ability to discriminate different land covers or material types is directly linked with the spectral resolution and sampling provided by the optical sensor. Several previous studies showed that the spectral resolution is a critical issue, especially to discriminate different land covers in urban areas. In spite of the increasing availability of hyperspectral data, multispectral optical sensors on board of several satellites are still acquiring everyday a massive amount of data with a relatively poor spectral resolution (i.e. usually about 4 to 7 spectral bands). These remotely sensed data are intensively used for Earth observation regardless of their limited spectral resolution. In this paper, we studied the ability of discrimination of several of these optical sensors: Pleiades, QuickBird, SPOT5, Ikonos, Landsat TM, Formosat and Meris. We used different spectral libraries which provide spectra of materials and land covers with a fine spectral resolution. These spectra were convolved with the Relative Spectral Responses (RSR) of each sensor to create spectra at the sensors' resolutions. Then, these reduced spectra were evaluated thanks to a separability index and machine learning tools. This study focuses on the ability of each sensor to discriminate different materials according to its spectral resolution. This approach allows us to fairly compare the different ability of the sensors to discriminate materials.

1. Introduction

The spectral resolution of a sensor can be characterized by the number of spectral bands, their associated bandwidths and their locations along the spectrum (Herold *et al.* 2003). Spectral resolution is also described by Lillesand and Kiefer (1994) as "the ability to discriminate fine spectral differences". Several previous studies (Herold *et al.* 2003, Meyer and Chander 2007, Heidena *et al.* 2007) showed that the spectral resolution is a critical issue, especially to discriminate different land covers in complex environment like urban areas. Most of multispectral systems have 4 to 7 spectral bands within the visible to middle infrared region of the electromagnetic spectrum. There exist however some systems that use one or more thermal infrared bands. One of the main benefits to use only multispectral versus hyperspectral acquisition, is the larger spatial coverage, which allows a faster and wider mapping of large areas. Indeed, satellite remote sensing systems provide both, a synoptic view space and economies of scale (Govender *et al.* 2007). Several satellites are now available on the market, each one offering specificities according to its sensors. Consequently, it is sometime difficult to choose a well suited sensor for a specific remote sensing application. To address this issue, simulation approaches can be

*Corresponding author. Email: germain.forestier@uha.fr

used in order to performed a theoric comparison of the ability of several sensors to discriminate fine spectral differences.

In this paper, we used several spectral libraries which contain spectra of materials and land covers with a fine spectral resolution. These spectra were extracted from the libraries and convolved with the Relative Spectral Responses (RSR) of several sensors to create coarser spectra at the sensors' resolutions. This work focuses on the ability of each sensor to discriminate different materials, according to its spectral resolution. As the spectra for each sensor are created from exactly the same spectra extracted from the libraries, the only variation is the RSR of the sensors. In this work, we only focus on comparing the spectral resolution of the sensors as we do not take into account the spatial resolution of the sensor, or other external factors (e.g. atmosphere, acquisition noire, etc.). While this choice limits the scope of this study, we believe that the insights provided by spectral comparison already bring an interessing knowledge about the discrimination ability of the studied sensors.

The rest of the paper is organized as follows. In Section 2, we present the sensor simulation approach along with related work. Then, in Section 3, we present the different spectral libraires that were used in the experiements. In Section 4, a class separability evaluation is presented. Experiments of classisication are detailed in Section 5. Finally, Section 6 concludes the paper.

2. Sensor simulation

2.1 *Previous work*

Sensor simulation, also called band simulation or band synthesis, consists in generating simulated multispectral spectra from data acquired by existing sensors, but with higher spectral resolution. The simulation consists in combining hyperspectral narrow bands into broader multispectral bands. This kind of approach has already been used, especially for sensor calibration and sensor simulation. The spectra simulation step uses the Relative Spectral Response (RSR) functions of the multispectral sensor, which describe the spectral response of each simulated sensor's band. For example, Green and Shimada (1997) used band synthesis for cross-calibration of a satellite multispectral instrument using AVIRIS data. The simulated data were used to determine the on-orbit radiometric calibration coefficients required for calibration of the spectral bands of the satellite.

A similar approach was used by Chander *et al.* (2004) for the cross-calibration of the Advanced Land Imager (ALI) from Landsat ETM+ well-calibrated data.

Salvatore *et al.* (1999) used band simulation to simulate the response of a new sensor from AVIRIS data. This simulation allowed the investigators to evaluate in advance the potentialities of the new multispectral sensor. This kind of simulation provides an opportunity to try variations in the original spectral response, and to adjust the RSR to achieve better results for the multispectral sensor objectives.

In another study, Jarecke *et al.* (2001) used Hyperion hyperspectral data to simulate Landsat ETM+ data and concluded that the difference between the simulated data and real data actually acquired by Landsat ETM+ was around 10%. Meyer and Chander (2007) used AVIRIS data to simulate MODIS and Landsat ETM+ data in order to illustrate how the differences in the RSR affect the observation of some typical surface features. The authors noticed some strong variations according to the different RSR. They concluded that more investigations were needed on how RSR affects the observation of different surfaces.

Concerning spectral indexes, Franke *et al.* (2006) used band simulation to compare the differences of the Normalized Difference Vegetation Index (NDVI) accord-

ing to the RSR of Landsat TM, Quickbird and SPOT5-HRV. The assessment of NDVI differences showed substantial variations between sensor systems. An inter-calibration approach using a polynomial order is suggested, to adjust NDVI differences caused by varying RSR functions. Polynomial corrections are also suggested for normalization. Trishchenko (2009) also studied the effects of RSR on surface reflectance and NDVI measured with moderate resolution satellite sensors. The results show more consistency between sensors with typical correction being under 5%. Another study of Teillet *et al.* (1997) demonstrates the impact of changes in RSR on NDVI derived from AVIRIS data. The results indicate that the NDVI is significantly affected by differences in spectral bandwidth, especially for the red band, and that changes in spatial resolution lead to less peruasive but more land cover specific effects on NDVI.

The use of the simulation to combine hyperspectral and multispectral images was studied by Kruse (2009). Hyperspectral data were used to extract endmembers, which were then simulated at multispectral resolution. These endmembers were then used to extend the hyperspectral mapping to the larger spatial coverage offered by the multispectral data.

The spectral resolution requirements for mapping urban areas was investigated by Herold *et al.* (2003). They used AVIRIS data and an urban spectral library to study the most suitable spectral bands for separating urban land cover types. The AVIRIS data were also used to simulate Landsat TM and Ikonos data. The results showed that Ikonos and Landsat TM lack of spectral details to efficiently map several urban classes.

More recently, Masunaga *et al.* (2010) proposed a satellite data simulator unit which provides a tool to perform simulation. They also present applications of sattelite simulation like model evaluation and algorithm development. Finally, Segl *et al.* (2010) also stressed the usefullness of remote sensig simulation for defining future Earth observation systems, optimizing instrument parameters, and developing and validating data-processing algorithms.

2.2 *Sensor simulation method*

To simulate multispectral data from hyperspectral data, the responses of narrow hyperspectral bands have to be aggregated. However, the reflectance values of the hyperspectral narrow bands cannot be summed directly to reproduce multispectral bands. Indeed, they must be weighted to account for the relative response of the multispectral bands. The RSR of each band of a sensor system is characterized by the effective spectral quantum efficiency, which indicates the spectral sensitivity of the band at each wavelength (Franke *et al.* 2006). Each sensor has consequently a different spectral sensitivity, which is described by its individual RSR functions. Figure 1 shows three examples of RSR functions for Quickbird, SPOT5-HRV and Landsat TM.

As stated by Clark *et al.* (2002), different strategies have been proposed to compute the weights to apply to each hyperspectral band. For the simulation used in this paper, each hyperspectral center wavelength was linked with the mean RSR value (in the range of the *full width half maximum* (FWHM) of the hyperspectral spectral band) of the simulated band. This approach is similar to the one proposed by Franke *et al.* (2006). The equation of the simulation of the reflectance L^{sim} according to the hyperspectral responses L and the RSRs values R for a band in the range (b_{min}, b_{max}) can be expressed as follows:

$$L^{sim}_{(b_{min},b_{max})} = \frac{\int_{b_{min}}^{b_{max}} L_\lambda R_\lambda \mathrm{d}\lambda}{\int_{b_{min}}^{b_{max}} R_\lambda \mathrm{d}\lambda} \quad (1)$$

One should notice that some external parameters are not simulated in this study. For example, some other simulation approaches (Kavzoglu 2004) take into account other aspects like atmospheric effects or geometric differences between sensors. In this study, we are interested in the sensor discrimination ability according to their RSR, that is why we only focused on spectral differences caused by different RSR functions. Other aspects like the spatial resolution should also be investigated and simulated to truly assess the differences between sensors. However, focusing only on spectral resolution already provides some insights on the different sensors ability.

Furthermore, we consider the used hyperspectral data as pure. Consequently, we did not apply other corrections (atmospheric corrections for example). As all simulations are made from the same spectra, the only variation in the simulation is the RSR functions of the sensors. This unique parameter variation approach allows us to fairly compare the different sensors.

3. Spectral librairies

3.1 *Available spectral libraries*

The advent of spectroscopy and remote sensing has offered an opportunity to develop a new kind of stored knowledge through spectral libraries. These spectral libraries are repositories of spectra of various kinds of materials (e.g. mineral, man-made material, vegetation, etc.) generally captured *in situ* using field instruments. Everybody agrees on the importance of the challenging problem to create such libraries in order to store, share and reuse information about materials. However, the number of freely available and easily accessible librairies is relatively limited. Indeed, an important number of factors limits their development, as the important cost of field acquisitions or the time needed to structure and organize the spectra in a meaningful way. In this section, we review the major available spectral libraries and their characteristics.

The most common and probably the most widely used library is the ASTER spectral library (Baldridge *et al.* 2008). This library includes contributions from the Jet Propulsion Laboratory (JPL), Johns Hopkins University (JHU) and the United States Geological Survey (USGS). It includes spectra of rocks, minerals, lunar soils, terrestrial soils, man-made materials, meteorites, vegetation, snow and ice covering the visible through thermal infrared wavelength region (0.4-15.4 μm). The first version was released in July 1998 and the second one is available since 2007 on simple request through the library website[1].

The USGS also offers its own library (Clark *et al.* 2007) which is freely available for download [2]. Researchers at the USGS Spectroscopy Lab have measured the spectral reflectance of hundreds of materials in the lab and have compiled a spectral library. This library contains over 1300 spectra organized in six groups: minerals, soils, coatings, liquid, man-made and plants. To the best of our knowledge these

[1] `http://speclib.jpl.nasa.gov`
[2] `http://speclab.cr.usgs.gov`

two libraries (ASTER and USGS) are the most comprehensive and freely available libraries.

Other smaller projects provide sometimes spectra, as for example the National Center for Geographic Information and Analysis (NCGIA) which offers a small library of urban spectra. The spectral library developed for this project contains over 130 averaged spectra from AVIRIS sensor structured in 7 urban classes. The library is available for download on the project website[1]. Herold *et al.* (2004) also created a library of more than 4500 individual urban spectra from the city of Santa Barbara categorized in 108 unique surface types. Another library of 270 spectra from AVIRIS data was also developped.

Several attempts to create platforms to store and to share spectra also exist. For example, Hueni *et al.* (2009) proposed a software named SPECCHIO[2], which is a tool to hold and structure reference spectra using a database. The authors make the distinction between spectral library (i.e. spectra list) and spectral database (i.e structured spectra with metadata). An interesting reflexion is discussed on the need to use standards and metadata.

Ferwerda *et al.* (2006) also offer a similar system through a website [3] where researchers can store and share their spectra. The German aerospace center (DRL) also provides a spectral archive website [4] with the intention to create a universal tool for archiving, managing and using spectra collected from various projects. Although these attempts to offer ways to share and store spectra are very interesting, they generally offer tools to structurate spectra but only provide few spectra. Furthermore, the multiplication of these tools tends to bring confusion to the user interested in creating and managing a spectral library. It is worth noticing that all these different libraries are structured following their own format, which increases the difficulty to gather information coming from various sources.

3.2 *Spectral libraries used in this study*

In this study, four different libraries were used to assess the discrimination ability of the different sensors. Table 1 summarizes the specifications of the different libraries and the description of each library is given hereafter.

- **ASTER/JHU** : We chose to use the spectra from the JHU of the ASTER spectral library as they offer an interesting class hierarchy as well as useful wavelength range for spectra simulation.
- **USGS** : We used the spectra from USGS library which are defined in the [0.35;2.5] μm range. Indeed, a certain number of spectra, especially mineral ones, are defined in the thermal channel, which are not used for most of the multispectral sensors.
- **NCGIA** : We used all the available spectra.
- **HEROLD** This spectral library contains around 1000 spectra of urban materials structured in four different levels. This library comes from an AVIRIS flight over the Santa Barbara city in 2001. This library has already been used in (Herold *et al.* 2003, 2004) to study the spectral requirement for mapping urban areas.

[1] `http://ncgia.ucsb.edu`
[2] `http://www.specchio.ch`
[3] `http://www.hyperspectral.info`
[4] `http://www.cocoon.caf.dlr.de`

4. Evaluation

4.1 *Class separability evaluation*

4.1.1 **Classical separability criteria.** Separability criteria aim at evaluating the separability of the classes of a dataset in a given feature space (Davis and Swain 1978). Different criteria have been proposed in the literature to evaluate and quantify this separability. For remote sensing applications, the divergence criterion (D), the transformed divergence criterion (TD), the Bhattacharyya distance (B) and the Jeffreys-Matusita distance (JM) are the most widespread criteria. These criteria have been mainly used in feature selection problems, where the goal is to select the best subset of 'informative' or 'relevant' features for a given dataset, in order to maximize classification accuracy for this reduced number of features.

In multispectral and hyperspectral image classification, these criteria were used to select the best subset of bands (De Backer *et al.* 2005, Mi-Hyun and K. 2008, Riedmann and Milton 2003). Indeed, some bands may be noisy or correlated, and consequently provide a misleading information about class separability. Ranson *et al.* (2003) also used the JM distance to compare the separability of the same thematic classes in two different images, an optical one and a radar one. This study was carried out to choose which image was the best suited to identify these classes. Assuming a Gaussian distribution, these criteria use the mean and the covariance matrix of the classes. Their definitions are given hereafter.

Divergence

$$\begin{aligned} D_{(i,j)} = & \tfrac{1}{2}\mathrm{tr}\left[(\Sigma_i - \Sigma_j)(\Sigma_i^{-1} - \Sigma_j^{-1})\right] \\ & + \tfrac{1}{2}\mathrm{tr}\left[(\Sigma_i^{-1} - \Sigma_j^{-1})(\mu_i - \mu_j)(\mu_i - \mu_j)^T\right] \end{aligned} \tag{2}$$

with μ_i and μ_j the means of the classes i and j, Σ_i and Σ_j the covariance matrices and $\mathtt{tr}[.]$ the trace of the matrix.

In the definition of the divergence (Eq.2) the second term on the right-hand side will increase continuously with the standard distance between the means of the pair of classes, thus the divergence will increase continuously with the standard distance between the means of the pair of classes. To solve this problem, a negative exponential term was introduced to transform the divergence (Bo *et al.* 2005). Thus, the transformed divergence (TD) is defined as a saturated version of the divergence.

Transformed divergence

$$TD_{(i,j)} = 2\left(1 - e^{-\frac{1}{8}D_{(i,j)}}\right) \tag{3}$$

The transformed divergence ranges in $[0; 2]$. Values in [0.0;1.0] indicate a very poor class separability, in [1.0;1.9] a poor separability and in [1.9;2.0] a relatively good separability.

Bhattacharyya distance

$$\begin{aligned} B_{(i,j)} = & \tfrac{1}{2}[\mu_i - \mu_j]^T \left[\frac{\Sigma_i + \Sigma_j}{2}\right]^{-1} [\mu_i - \mu_j] \\ & + \tfrac{1}{2}\mathtt{ln}\frac{\left|\frac{1}{2}[\Sigma_i + \Sigma_j]\right|}{\sqrt{|\Sigma_i||\Sigma_j|}} \end{aligned} \tag{4}$$

The Bhattacharyya distance, as the divergence, is unbounded. To cope with this problem, the Bhattacharyya distance is used in the Jeffreys-Matusita distance with a negative exponential term.

Jeffreys-Matusita distance

$$JM_{(i,j)} = \sqrt{2(1 - e^{-B_{(i,j)}})} \tag{5}$$

The Jeffreys-Matusita distance ranges in $[0; 2]$ and the ranges of interpretation are barely similar to those of the transformed divergence.

4.1.2 **Extension to multiclass problems.** The criteria defined in the previous section are designed to evaluate the separability between a couple of classes. To extend those to multiclass problems, different approaches have been proposed (Bruzzone *et al.* 1995, Bruzzone and Serpico 2000). The most common strategy is to use the average or the weighted average distances computed for all pairs of classes.

$$JM_{avg} = \frac{C(C-1)}{2} \sum_{i=1}^{C-1} \sum_{j=i+1}^{C} JM_{(i,j)} \tag{6}$$

$$TD_{avg} = \frac{C(C-1)}{2} \sum_{i=1}^{C-1} \sum_{j=i+1}^{C} TD_{(i,j)} \tag{7}$$

These means can be weighted to take into account the class prior probability $p(\omega)$:

$$JM_{wavg} = \sum_{i=1}^{C} \sum_{j>i}^{C} p(\omega_i)p(\omega_j)JM_{(i,j)} \tag{8}$$

$$TD_{wavg} = \sum_{i=1}^{C} \sum_{j>i}^{C} p(\omega_i)p(\omega_j)TD_{(i,j)} \tag{9}$$

Another formulation, which better approximates the Bayes error using Jeffreys-Matusita distance, is given by Bruzzone and Serpico (2000):

$$JM_{wavg} = \sum_{i=1}^{C} \sum_{j>i}^{C} \sqrt{p(\omega_i)p(\omega_j)}JM^2_{(i,j)} \tag{10}$$

$$TD_{wavg} = \sum_{i=1}^{C} \sum_{j=1}^{C} p(\omega_i)p(\omega_j)TD_{(i,j)} \tag{11}$$

Alternatively, the minimum Jeffreys-Matusita distance is sometimes used to evaluate the minimum distance between a couple of classes among a set of classes. It evaluates the minimum separability among the classes and can be used as an indicator of separability of the whole dataset.

$$JM_{min} = \texttt{min}(JM_{(i,j)}) \quad \forall i, j \in [1 \dots C] \quad i \neq j \tag{12}$$

An intensive work is still under progress, mainly in the fields of pattern recognition and data mining, to propose new criteria to solve the features selection problem. Recent works use information theory and subspace analysis to design new criteria (Guo *et al.* 2008, Lai *et al.* 2006, Sotoca *et al.* 2007, Gunala and Edizkanb 2008, Liua *et al.* 2009). However, the criteria presented in this section are the most commonly used, especially in the remote sensing field. An exhaustive presentation of all criteria is out of scope of this paper.

The choice between Jeffreys-Matusita distance and the divergence to evaluate the separability of a set of classes is not trivial. Richards and Jia (2006) claim that Jeffreys-Matusita distance tends to perform better as a feature selection criterion than the divergence, but is computationally more complex. This is mainly due to the high number of matrix operations required to compute the Bhattacharyya distance. The Jeffreys-Matusita distance and the transformed divergence are described as almost as effective and considerably better than simple divergence and simple Bhattacharyya, essentially thanks to their bounded range. The Jeffreys-Matusita distance and the transformed divergence seem equally used in the literature without clear arguments on why choosing one or the other. In this paper we chose to use the Jeffreys-Matusita distance.

4.2 *Classification accuracy*

Another way of evaluating class separability and assessing features relevance is to perform a supervised classification of the dataset. The accuracy and the confusion matrix of the classification are useful tools to assess the quality of features. Indeed, as stated by Heidena *et al.* (2007), separability criteria can suffer from some problems in extreme cases. For example, a class can show a good separability with the other classes with a constant overlap of 5% for each class in the feature space. However, the total spectral overlap can range from 5% allowing a classification of good quality to 100% making the accurate classification of this material impossible. Furthermore, the computation of the Bhattacharyya distance requires the calculation of the inverse of the covariance matrix, which can be sometimes problematic. Indeed, when the number of features increases, the covariance matrix tends to become singular and consequently not invertible.

To evaluate the classification performance on the spectral libraries we used an ensemble classifier system (Kittler *et al.* 1998), which combines three different supervised methods: a 1-Nearest-Neighbour classifier, a Naive Bayes classifier, and a C4.5 classifier. These classifiers were combined through a majority voting strategy. This choice has been made to reduce the bias involved in the selection of a single algorithm. For the experiment, 10-cross-validation has been used. It consists in splitting the dataset in 10 subsets and then, in learning on $\frac{9}{10}$ of the dataset and then evaluating on the remaining $\frac{1}{10}$. The evaluation is computed for all the combinations. This approach avoids to split the dataset in a learning set and an evaluation set and is statistically more relevant (as each sample is used alternatively for learning and testing).

5. Experiments

In this section, we present three different experiments carried out to illustrate the usefulness of sensor simulation. Table 2 summarizes the information on the sensors used in the experiments, which are some of the most common multispectral systems available.

In the first experiment (Section 5.1), we compared the different sensors according to their spectral response defined by their RSR function. The different libraries presented in Section 3. were convolved with the RSR of each sensor. Then, separability index and classification accuracy were computed in order to compare the different sensors. Hence, we were able to gain some insight on the sensor ability to classify materials accurately. Furthermore, the comparison is fair as the dataset for each sensor is created from the exact same spectral libraries. The only variation for each dataset is the RSR used to convolve the spectra.

The second experiment (Section 5.2), consisted in evaluating the potential interest of spectral indexes (e.g., NDVI). The aim of this simulation was to evaluate if a specific spectral index is useful for the classification of a specific material, and if the sensors were able to leverage this new information. Classification accuracy assessment and separability evaluation were conducted with and without the use of spectral indexes in order to evaluate the interest of their addition to the dataset.

The last experiment (Section 5.3) illustrates one of the many potential uses of sensor simulation. In this experiment, we evaluated the interest of a specific band, namely the Short-Wave Infra-Red band (SWIR). To study the usefulness of this band we carried out two evaluations: the first one consisted in removing the SWIR band from a sensor equipped of this band, when the second one consisted in adding this band to a sensor not originally equipped. This experiment reveals how sensor simulation can be used to design new sensors and evaluate the interest of a specific spectral band.

5.1 *Sensors evaluation and comparison*

In this first experiment the different libraries were used to compare the different sensors. The results are presented in Table 3 where the accuracy of the ensemble classifier is presented in the column Vote, and the Jeffreys-Matusita distance in the column JM. We discuss the results for each dataset hereafter.

ASTER : The results for this data set are presented in Tab. 4. The Ikonos and Formosat-2 sensors give the lowest results. This is consistent as they have a low spectral resolution compared to the other studied sensors. They are followed by Spot 5-HRV, Quickbird and Pleiades and finally Meris which achieves the best results. An interesting point to notice in these results is the relative large difference between the accuracy of Quickbird (84.4%) and Pleiades (92.2%). As these two sensors have the same number of bands which are very similar, one could expect a similar behaviour in classification accuracy. However, even if the RSR are strongly similar, there are still some small variations. The most important difference in the bands of these two sensors is the Near Infra Red (NIR) band. To check if the difference of accuracy was due to this difference of RSR, we removed the NIR band of these two sensors and ran the classification again. This time, the accuracies were quite close with 83.3% for Pleiades and 81.5% for Quickird. Then, we replaced the NIR band of Quickbird by the NIR band of Pleiades to check if the NIR band of Pleiades was truly responsible of the higher accuracy. We obtained this time 92.2% for Pleiades and 91.1% for Quickbird (instead of 84.4% with its own NIR band). These results supported our hypothesis that the variation in the NIR band was

responsible of the difference of accuracy.

We investigated more closely the results to identify some examples where Pleiades was able to correctly discriminate two specific spectra, while Quickbird was not. We identified several couples of spectra misclassified by Quickbird and well classified by Pleiades. We present here a example with a Asphalt spectrum (Man-Made) and a Basalt spetrum (Rocks) (see Figure 3 (a)). On Figure 3 (b), one can observ that the NIR bands of the two sensors are quite similar, but not exactly defined in the same range of wavelengths. This small shift on the wavelength seems to be responsible of the difference of accuracy. On Figure 3 (c), one can clearly see that the two spectra are very close in the range of the Quickbird NIR band while they seem to be more separable in the Pleiades NIR band range.

These results are consistent with previous studies which also pointed out that even small variations in band definition can imply differences in spectral response of some materials. For example, in Franke *et al.* (2006), the authors showed that the variation on the NIR band of different sensors leads to strong variation in the calculation of the NDVI. In Meyer and Chander (2007), the authors showed that the definition of the RSR is a key issue to allow the identification of some type of materials. The conclusion from these results is not that Pleiades is better than Quickbird, but rather than even two sensors having similar bands can produce different results according to the application. Furthermore, these differences might be estimated and evaluated thanks to sensors simulation as in the present study. Figure 4 presents the accuracy of each class at each level for each sensor.

USGS : The results for the USGS data set are consistent with the spectral resolution of the sensor (see Tab. 5). The best results are achieved by Landsat and Meris with an accuracy of 79.5%. It seems that the Landsat bands are especially well suited for this data set and helps to better discriminate several spectra confused by the other sensors.

NCGIA : In this data set, the best results are achieved by SPOT 5-HRV sensor. The SWIR channel seems useful in this application to discriminate some urban land covers like *Road* and *Roof*, which are well known as difficult to classify. The Tab. 6 presents the results for the different sensors and the Figure 5 the accuracy for each class.

Herold : One of the interesting things to observe in the results of this data set, is the behavior of the sensors according to the level of classification. Indeed, this data set comes with a class hierarchy of four levels. The classification is expected to be more difficult as the number of classes increases, since the probability of confusion between the classes increases as well. In levels I and II the results are barely similar among the different sensors with an accuracy around 96% for level I and 91% for level II. However, at level III, some differences of accuracy appear and again, the sensors with better spectral resolution have better results. Landsat has particularly good results with an accuracy of 91.4% followed by Meris with 88.3%. The trend is maintained on level IV. This kind of experiment allows us to gain some insight on the ability of the sensors to map land cover at certain levels. If a user is interested in mapping some general classes (Level I and II), the choice of the sensor is not crucial. However, if the user is interested in mapping specific classes deeper in the hierarchy (Level III and IV), the user should carefully select a sensor which accurately maps these classes.

5.2 *Spectral index assessment*

Spectral indexes are non linear combinations of bands which are used to highlight some specific features in images (vegetation, soil, buildings, water, ...). Simulation

can be used to evaluate if the addition of a spectral index improves the separability of the classes along with the classification accuracy. We give in this section a simple example with the well-known *Normalized Difference Vegetation Index* (NDVI). We classified the dataset generated for Ikonos, Pleiades, Quickbird and Spot 5-HRV with and without the addition of the NDVI.

The results presented in Table 8 reveal that the addition of the NDVI tends to increase the classification accuracy for most of the datasets but not for all (e.g. NCGIA). In this experiment, Spot 5-HRV does not seem to leverage the information provided by the NDVI, except for the Herold dataset where the NDVI seems informative for all the sensors.

5.3 *Spectral band removal/addition assessment*

Simulation can also be used to evaluate if the addition of a band to a sensor is relevant for a certain type of application. It allows to evaluate in advance the potentialities of the new multispectral sensor, and provide an opportunity to try variations in the original spectral response, and to adjust the RSR to achieve better results for the multispectral sensor objectives.

To illustrate this, we choose to evaluate how the Pleiades sensor reacts to the addition of the Short-Wave Infra Red band (SWIR) and how the Spot 5-HRV sensor reacts to its removal. The results are presented in Table 9. The addition of the SWIR band to Pleiades sensor does not seem to improve the results in this specific experiment. However its removal to the Spot 5-HRV sensor greatly influences the classification results as the accuracy are always lower without this band. These results can help to design or adjust the definition of spectral bands for future sattelites programm.

6. Conclusion

In this study, we presented how sensor simulation could be used to evaluate the ability of a sensor to discriminate spectral variation of land covers and materials. This simulation consisted in converting precise spectra extracted from spectral libraries into spectra at a coarser resolution. Some of the most common multispectral sensors were simulated. A comparison using the transformed spectra was performed to assess their ability to discriminate and classify different land covers and materials. The presented results provide important insights on sensor discrimination abilities according to their Relative Spectral Response (RSR). Furthermore, different ways to use the simulation to compare and understand differences between sensors were presented. For example, we showed that small differences in the definition of a band can lead to very different results (Sect 5.1). We also highlighted that depending on the level of details (e.g. number of classes to differenciate), some sensors were more recommended than otherss (Sect 5.1). We also showed that the potential improvement of classification accuracy using a spectral index (e.g. NDVI) could be evaluated through simulation (Sect 5.2). Along with helping to understand existing sensors, we highlighted that simualtion could be used to help creating new ones 5.3. Indeed, the tedious process of sensor design could be greatly backed by early simulation which could help to design specific RSR.

The results presented in this study have to be balanced by the relative low number of spectra present in the used datasets and their relevance for different applications. Indeed, spectral libraries are expensive to develop and consequently, are rarely freely distributed Furthermore, it is worth noticing that the simulation

presented in this study did not take into account several important factors like the impact of atmosphere, the spatial resolution of the sensor, the mixture of spectra, the acquisition noise, etc. Indeed, remote sensing images often exhibit mixed pixels which are composed of a mixture of several pure spectra plus some noice. While this study does not adress directly this issue, it provides a first comparison of sensor discrimination ability focusing only on spectral differences. Further work is necessary to improve the simulation task to take into account more parameters in order to be closer to the reality and the complexity of remote sensing data. However, this kind of simulation is still an unexplored wilderness and possesses a great potential for various applications.

.

References

Baldridge, A.M., Hook, S.J., Grove, C.I. and Rivera, G., 2008, The ASTER Spectral Library Version 2.0. *Remote Sensing of Environment*.

Bo, Y., Wang, J. and Li, X., 2005, Exploring the scale effect in land cover mapping from remotely sensed data: the statistical separability-based method. *International Geoscience and Remote Sensing Symposium*.

Bruzzone, L., Roli, F. and Serpico, S.B., 1995, An extension of the Jeffreys-Matusita distance to multiclass cases for feature selection. *IEEE Transactions on Geoscience and Remote Sensing*, **33**, pp. 1318–1321.

Bruzzone, L. and Serpico, S.B., 2000, A technique for feature selection in multiclass problems. *International Journal of Remote Sensing*, **21**, pp. 549–563.

Chander, G., Meyer, D. and Helder, D., 2004, Cross calibration of the Landsat-7 ETM+ and EO-1 ALI sensor. *IEEE Transactions on Geoscience and Remote Sensing*, **42**, pp. 2821–2831.

Clark, R., Swayze, G., Wise, R., Livo, E., Hoefen, T., Kokaly, R. and Sutley, S., 2007, USGS digital spectral library splib06a. *U.S. Geological Survey, Digital Data Series 231*.

Clark, R.N., Swayze, G.A., Livo, K.E., Kokaly, R.F., King, T.V.V., Dalton, J.B., Vance, J.S., Rockwell, B.W., Hoefen, T. and McDougal, R.R., 2002, Synthesis of Multispectral Bands from Hyperspectral Data: Validation Based on Images Acquired by AVIRIS, Hyperion, ALI, and ETM+. *AVIRIS Workshop*.

Davis, S.M. and Swain, P.H., 1978, *Remote Sensing: The Quantitative Approach* (McGraw-Hill International Book Company).

De Backer, S., Kempeneers, P., Debruyn, W. and Scheunders, P., 2005, A band selection technique for spectral classification. *Geoscience and Remote Sensing Letters, IEEE*, **2**, pp. 319–323.

Erdas, 1999, *Erdas Field Guide* (Erdas, Inc., Atlanta, GA).

Ferwerda, J.G., Jones, S.D. and Reston, M., 2006, A free online reference library for hyperspectral reflectance signatures. *SPIE Newsroom*.

Franke, J., Heinzel, V. and Menz, G., 2006, Assessment of NDVI- Differences Caused by Sensor Specific Relative Spectral Response Functions. *IEEE International Geoscience and Remote Sensing Symposium*, pp. 1138–1141.

Govender, M., Chetty, K. and Bulcock, H., 2007, A review of hyperspectral remote sensing and its application in vegetation and water resource studies. *Water SA*, **33**, pp. 145–152.

Green, R.O. and Shimada, M., 1997, On-orbit calibration of a multi-spectral

satellite sensor using a high altitude airborne imaging spectrometer. *Advances in Space Research*, **19**, pp. 1387–1398.

Gunala, S. and Edizkanb, R., 2008, Subspace based feature selection for pattern recognition. *Information Sciences*, **178**, pp. 3716–3726.

Guo, B., Damper, R.I., Gunn, S.R. and Nelson, J.D.B., 2008, A fast separability-based feature-selection method for high-dimensional remotely sensed image classification. *Pattern Recognition*, **41**, pp. 1653–1662.

Heidena, U., Segl, K., Roessner, S. and Kaufmann, H., 2007, Determination of robust spectral features for identification of urban surface materials in hyperspectral remote sensing data. *Remote Sensing of Environment*, **111**, pp. 537–552.

Herold, M., Gardner, M. and Roberts, D., 2003, Spectral resolution requirements for mapping urban areas. *IEEE Transactions on Geoscience and Remote Sensing*, **41**, pp. 1907–1919.

Herold, M., Roberts, D.A., Gardner, M.E. and Dennison, P.E., 2004, Spectrometry for urban area remote sensing : Development and analysis of a spectral library from 350 to 2400 nm. *Remote Sensing of Environment*, **91**, pp. 304–319.

Hueni, A., Nieke, J., Schopfer, J., Kneubhler, M. and Itten, K., 2009, The spectral database SPECCHIO for improved long-term usability and data sharing. *Computers & Geosciences*, **35**, pp. 557–565.

Jarecke, P., Barry, P., Pearlman, J. and Markham, B., 2001, Aggregation of Hyperion hyperspectral spectral bands into Landsat-&ETM+ spectral bands. *IEEE International Geoscience and Remote Sensing Symposium*, **6**, pp. 2822–2824.

Kavzoglu, T., 2004, Simulating Landsat ETM+ imagery using DAIS 7915 hyperspectral scanner data. *International journal of remote sensing*, **25**, pp. 5049–5067.

Kittler, J., Hatef, M., Duin, R.P.W. and Matas, J., 1998, On Combining Classifiers. *IEEE Transaction on Pattern Analysis and Machine Intelligence*, **20**, pp. 226–239.

Kruse, F.A., 2009, Improving multispectral mapping by spectral modeling with hyperspectral signatures. *Journal of Applied Remote Sensing*, **3**.

Lai, C., Reinders, M.J.T. and Wessels, L., 2006, Random subspace method for multivariate feature selection. *Pattern Recognition Letters*, **27**, pp. 1067–1076.

Lillesand, T.M. and Kiefer, R.W., 1994, *Remote Sensing and Image Interpretation* (John Wiley & Sons).

Liua, H., Sun, J., Liua, L. and Zhang, H., 2009, Feature selection with dynamic mutual information. *Pattern Recognition*, **42**, pp. 1330–1339.

Masunaga, H., Matsui, T., Tao, W., Hou, A., Kummerow, C., Nakajima, T., Bauer, P., Olson, W., Sekiguchi, M. and Nakajima, T., 2010, Satellite Data Simulator Unit (SDSU): A multi-sensor, multi-spectral satellite simulator package. *Bulletin of the American Meteorological Society.*

Meyer, D. and Chander, G., 2007, The effect of variations in relative spectral response on the retrieval of land surface parameters from multiple sources of remotely sensed imagery. *IEEE International Geoscience and Remote Sensing Symposium*, pp. 5150–5153.

Mi-Hyun, P. and K., S.M., 2008, Classifying environmentally significant urban land uses with satellite imagery. *Journal of Environmental Management*, **86**, pp. 181–192.

Ranson, K.J., Kovacs, K., Sun, G. and Kharuk, V.I., 2003, Disturbance

recognition in the boreal forest using radar and Landsat-7. *Canadian Journal of Remote Sensing*, **29**, pp. 271–285.

Richards, J.A. and Jia, X., 2006, *Remote Sensing Digital Image Analysis*, Springer .

Riedmann, M. and Milton, E., 2003, Supervised band selection for optimal use of data from airborne hyperspectral sensors. *IEEE Geoscience and Remote Sensing Symposium*, **3**, pp. 1770–1772.

Salvatore, E., Esposito, C., Krug, T. and Green, R., "Simulation of the Spectral Bands of the CDD and WFI Cameras of the CBERS Satellite using AVIRIS Data", 1999.

Segl, K., Guanter, L., Kaufmann, H., Schubert, J., Kaiser, S., Sang, B. and Hofer, S., 2010, Simulation of spatial sensor characteristics in the context of the EnMAP hyperspectral mission. *IEEE Transactions on Geoscience and Remote Sensing*, **48**, pp. 3046–3054.

Sotoca, J., Pla, F. and Sanchez, J., 2007, Band Selection in Multispectral Images by Minimization of Dependent Information. *IEEE Transactions on Systems, Man, and Cybernetics, Part C: Applications and Reviews*, **37**, pp. 258–267.

Teillet, P., Staenz, K. and William, D., 1997, Effects of spectral, spatial, and radiometric characteristics on remote sensing vegetation indices of forested regions. *Remote Sensing of Environment*, **61**, pp. 139 – 149.

Trishchenko, A.P., 2009, Effects of spectral response function on surface reflectance and NDVI measured with moderate resolution satellite sensors: Extension to AVHRR NOAA-17, 18 and METOP-A. *Remote Sensing of Environment*, **113**, pp. 335 – 341.

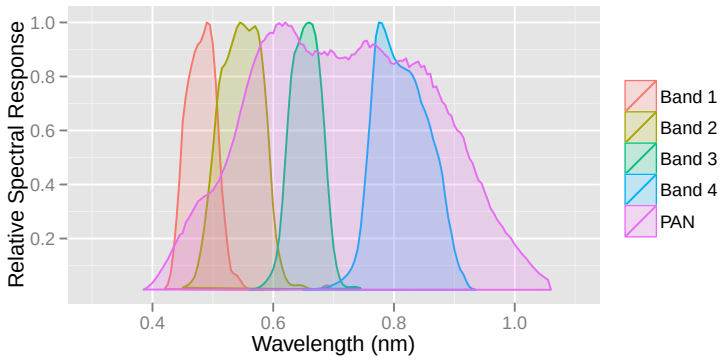

(*a*) Quickbird

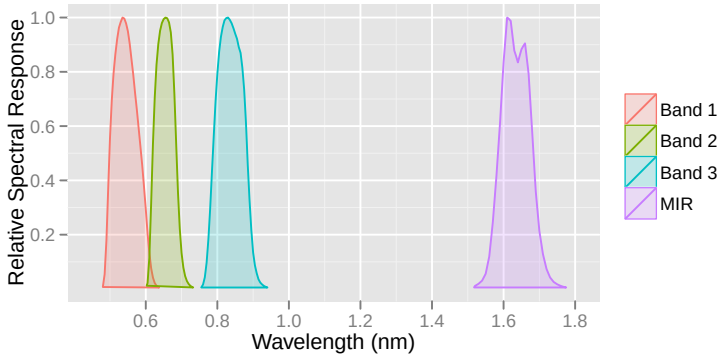

(*b*) SPOT5-HRV

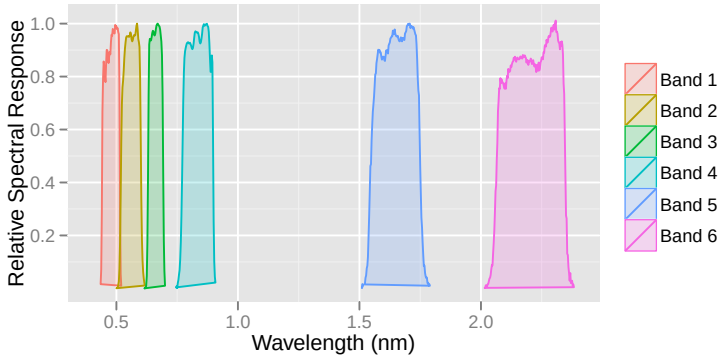

(*c*) Landsat TM

Figure 1. Example of RSR functions of three sensors namely, (a) Quickbird; (b) SPOT5-HRV and (c) Landsat TM.

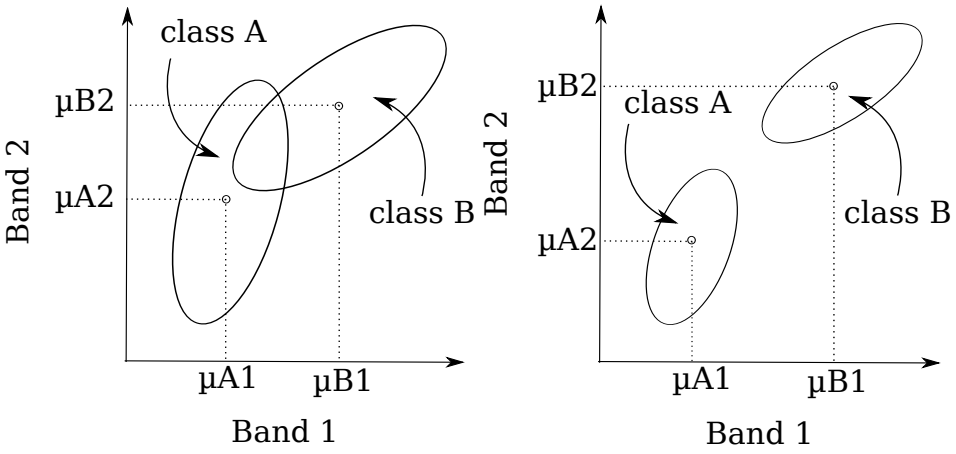

(*a*) Overlapping classes imply bad separability

(*b*) Good separability

Figure 2. Illustration of the class separability problem (Erdas 1999).

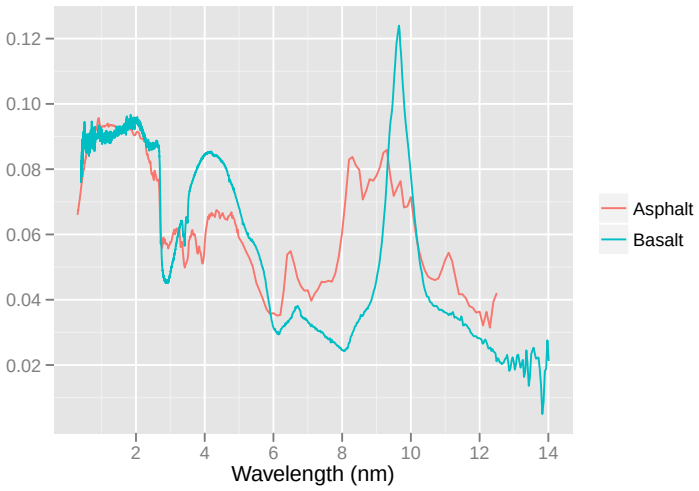

(*a*) Asphalt and Basalt spectra

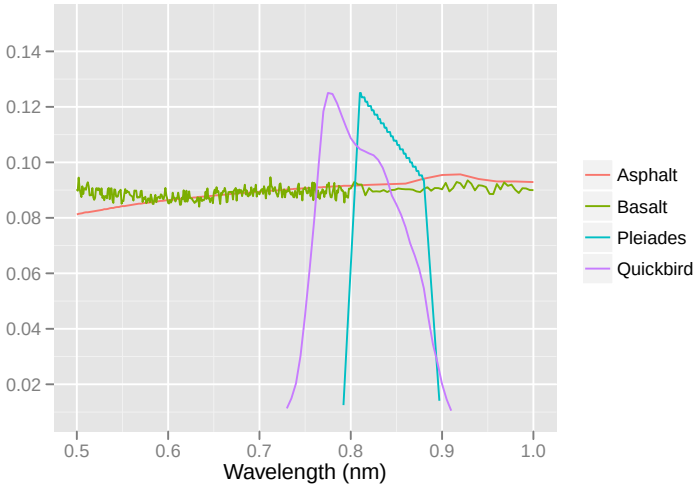

(*b*) Zoomed Asphalt and Basalt spectra and the NIR band of Quickbird and Pleiades

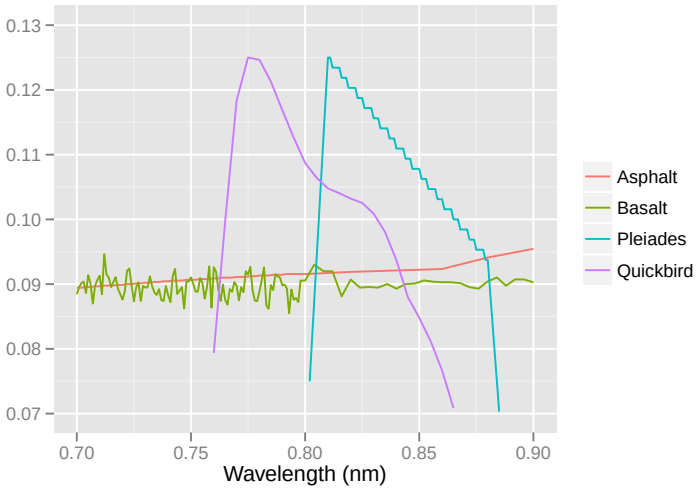

(*c*) Zoomed Asphalt and Basalt spectra and the NIR band of Quickbird and Pleiades

Figure 3. Asphalt (Man-Made), Basalt (Rocks) (a) and the NIR bands of Quickbird and Pleiades (c)

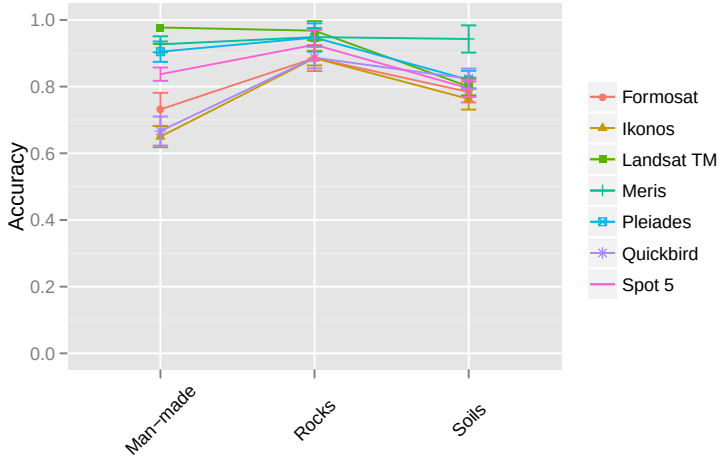

(*a*) Level 1

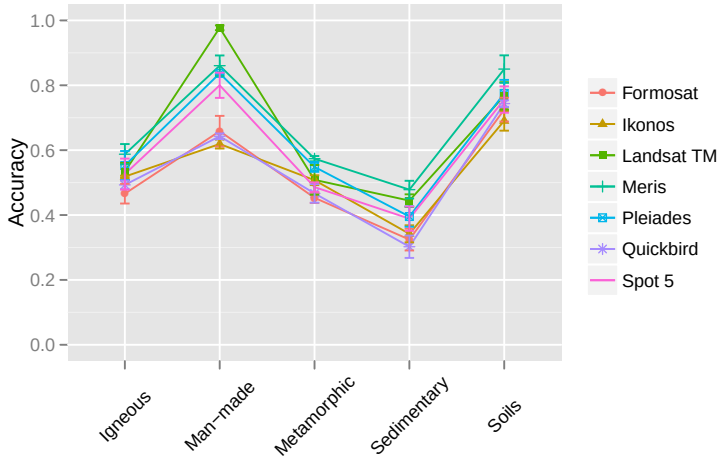

(*b*) Level 2

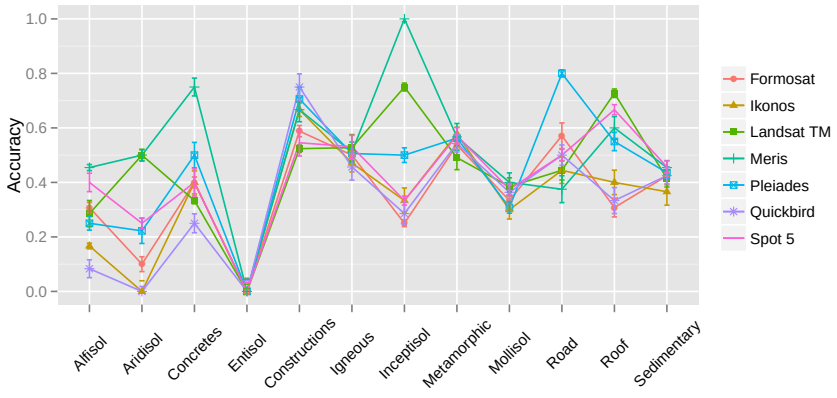

(*c*) Level 3

Figure 4. Classification accuracy per class for ASTER/JHU Level 1 (a), Level 2 (b) and Level 3 (c).

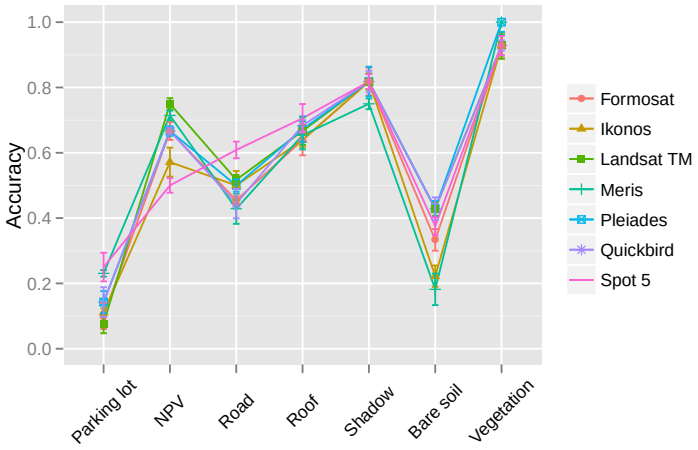

Figure 5. Classification accuracy per class for NCGIA

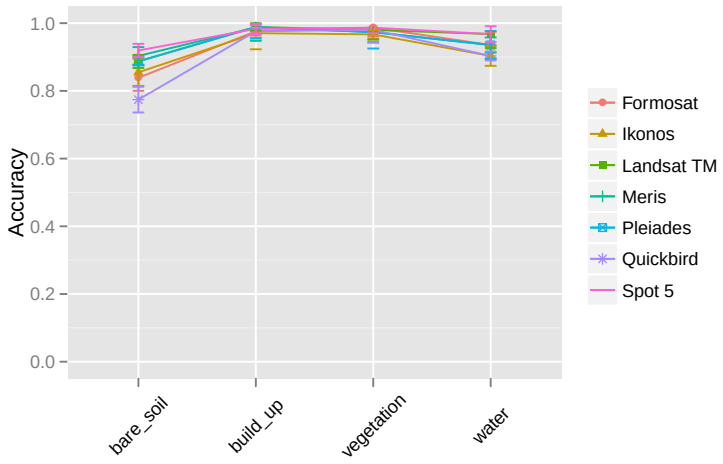

(*a*) Level 1

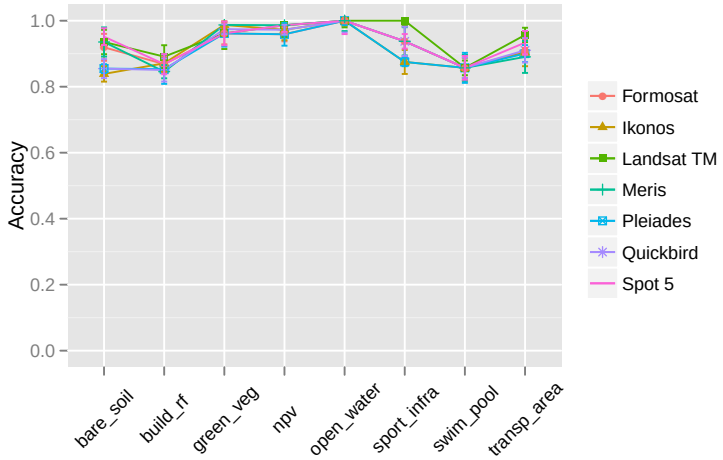

(*b*) Level 2

Figure 6. Classification accuracy per class for HEROLD Level 1 (a) and Level 2 (b)

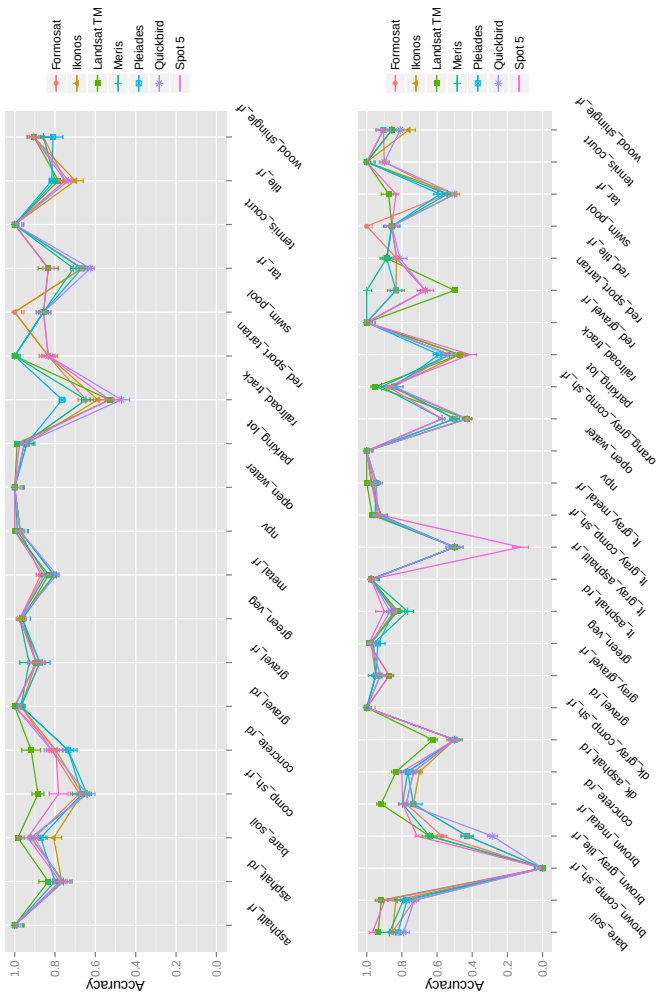

(*a*) Level 1 (*b*) Level 2

Figure 7. Classification accuracy per class for HEROLD Level 3 (a) and Level 4 (b)

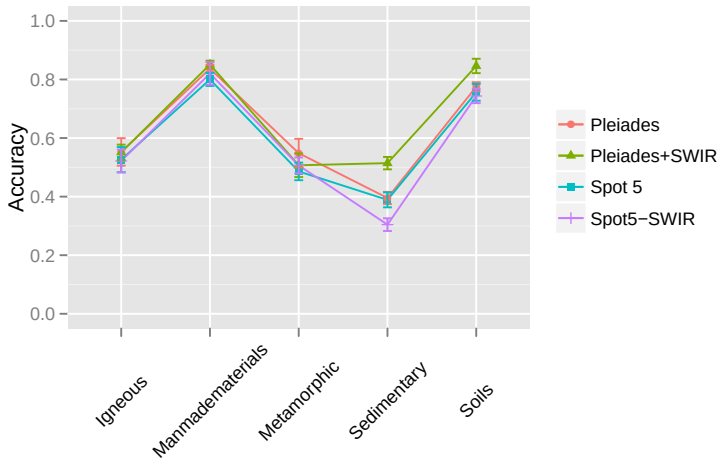

(*a*) Classification accuracy per class for ASTER/JHU Level 2

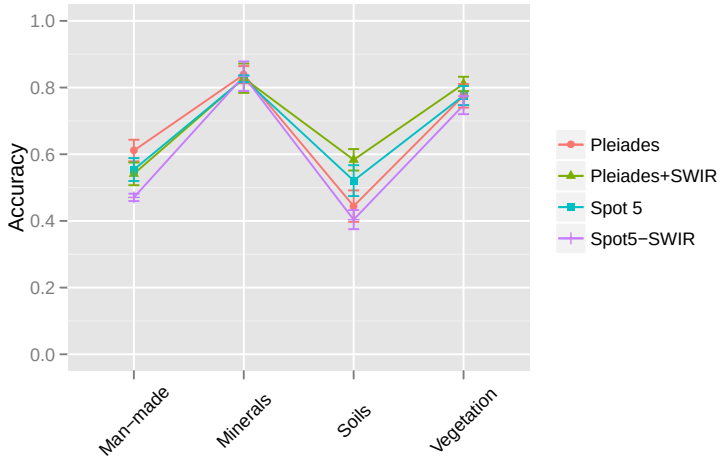

(*b*) Classification accuracy per class for USGS

Figure 8. Influence of adding/removing the SWIR channel to Pleiades and SPOT5 on the classification accuracy.

Table 1. Spectral libraries used in this study.

	# Classes for each level	# Spectra	# Levels	Instrument	Wavelength range
ASTER/JHU	3/5/12	270	3	Beckman/Nicolet	[0.4;14.0] μm
ASTER/JPL	6/20	283	2	Beckman/Nicolet	[14;0.4] μm
USGS	4	860	1	Beckman/ASD/Nicolet	[0.35;2.5] μm
NCGIA	7	133	1	AVIRIS	[0.37;2.5] μm
HEROLD	4/8/19/26	956	4	AVIRIS	[0.37;2.5] μm

Table 2. Information about the different sensors included in this study.

Name	# Bands	# Owner	# Bands
Spot 5-HRV	4	CNES	
Quickbird	5	Digital Globe	[0.50; 0.59] [0.61; 0,68] [0.78; 0.89] 20m x 20m [0.50; 0.73] 10m x 10m
Pleiades	5	CNES	[0.45; 0.52] [0,52; 0,60] [0,63; 0,69] [0,76; 0,90] 2,44 x 2,44 m [0.445; 0.900] 0.61 m x 0.61 m
Landsat TM	6	NASA	[0,45; 0,52] [0,52; 0,60] [0,63; 0,69] [0,76; 0,90] [1,55; 1,75] [2,08; 2,35] 30 m x 30 m [10,4; 12,5] 120 x 120 m
Ikonos	4	Space Imaging Corporation	[0,45; 0,52] [0,52; 0,60] [0,63; 0,69] [0,76; 0,90] 4 x 4 m
Formosat-2	5	Taiwan	[0,45; 0,52] [0,52; 0,60] [0,63; 0,69] [0,76; 0,90] [0,45; 0,90]
Meris	15	ESA	[0.4125] $\pm$ 10 [0.4425] $\pm$ 10 [0.490] $\pm$ 10 [0.510] $\pm$ 10 [0.560] $\pm$ 10 [0.620] $\pm$ 10 [0.665] $\pm$ 10 [0.68125] $\pm$ 7.5 [0.70875] $\pm$ 10 [0.75375] $\pm$ 7.5 [0.760625] $\pm$ 3.75 [0.77875] $\pm$ 15 [0.865] $\pm$ 20 [0.885] $\pm$ 10 [0.900] $\pm$ 10

Table 3. Sensors comparison on all the available datasets.

Library	Ikonos		Pleiades		Quickbird		Formosat-2		Landsat		Spot 5-HRV		Meris	
	JM	Vote	JM	Vote	JM	Vote	JM	Vote	JM	Vote	JM	Vote	JM	Vote
Aster I	0,79	83,3	0,82	92,2	0,76	84,4	0,76	84,8	0,85	94,4	0,76	89,2	0,92	94,4
Aster II	1,20	53,3	1,21	61,1	1,23	51,4	1,16	51,1	1,29	62,5	1,16	57,7	1,55	64,8
Aster III	1,31	45,1	1,29	50,0	1,31	44,8	1,28	45,9	1,33	48,8	1,26	50,7	1,60	51,8
NCGIA	1,38	59,3	1,38	62,4	1,39	61,6	1,38	60,1	1,41	60,9	1,37	63,1	0,76	56,8
USGS	0,84	77,0	0,86	77,6	0,84	75,9	0,84	76,4	0,92	79,5	0,86	77,5	1,21	79,5
Herold I	0,79	96,4	0,78	96,5	0,78	96,4	0,78	96,8	0,81	97,8	0,78	96,7	0,75	97,2
Herold II	1,28	91,5	1,26	91,8	1,30	90,5	1,23	91,7	1,31	93,3	1,29	91,6	0,89	92,2
Herold III	1,76	85,6	1,74	86,6	1,76	85,1	1,75	85,3	1,80	91,4	1,78	88,1	1,55	88,3
Herold IV	1,84	85,3	1,81	86,7	1,84	85,2	1,82	85,1	1,85	90,6	1,84	88,3	1,75	87,4

Table 4. ASTER/JHU.

Sensor	Level	JM_{wave}	JM_{ave}	JM_{min}	TD_{wave}	TD_{ave}	1NN	NaiveBayes	J48	Vote
Ikonos	I	0,796	1,780	1,531	0,884	1,922	82,963	58,519	80,370	83,333
-	II	1,204	1,584	0,938	1,394	1,780	53,333	41,852	48,889	53,333
-	III	1,312	1,836	0,320	1,495	1,976	44,074	32,963	37,407	45,185
Pleiades	I	0,825	1,825	1,599	0,878	1,912	92,593	62,593	86,296	92,222
-	II	1,212	1,597	0,978	1,341	1,726	60,741	46,296	54,074	61,111
-	III	1,293	1,772	0,128	1,447	1,956	47,778	35,185	42,222	50,000
Quickbird	I	0,761	1,729	1,540	0,884	1,921	83,704	59,259	81,111	84,444
-	II	1,237	1,616	1,004	1,455	1,858	52,593	41,852	47,037	51,481
-	III	1,314	1,765	0,446	1,546	1,985	42,222	32,593	37,037	44,815
Formosat-2	I	0,763	1,696	1,605	0,864	1,886	85,926	58,519	80,000	84,815
-	II	1,169	1,524	1,034	1,350	1,725	53,333	42,593	48,519	51,111
-	III	1,281	1,718	0,386	1,471	1,968	45,185	32,963	37,037	45,926
Landsat	I	0,858	1,882	1,721	0,926	1,994	94,815	85,556	91,852	94,444
-	II	1,296	1,698	0,928	1,469	1,887	62,222	57,778	60,000	62,593
-	III	1,335	1,732	0,370	1,537	1,984	49,259	41,481	37,778	48,889
Spot 5-HRV	I	0,761	1,727	1,504	0,901	1,951	90,000	71,481	84,074	89,259
-	II	1,161	1,529	0,760	1,348	1,747	60,000	50,370	50,370	57,778
-	III	1,268	1,747	0,308	1,433	1,949	48,148	35,926	43,704	50,741
Meris	I	0,924	1,992	1,975	0,929	2,000	94,444	60,000	88,889	94,444
-	II	1,557	1,982	1,925	1,572	2,000	64,815	50,370	58,519	64,815
-	III	1,602	1,943	1,169	1,636	2,000	52,963	35,926	43,333	51,852

Table 5. USGS

Sensor	JM_{wave}	JM_{ave}	JM_{min}	TD_{wave}	TD_{ave}	1NN	NaiveBayes	J48	Vote
Ikonos	0,840	1,309	0,706	1,063	1,709	73,140	57,791	74,302	77,093
Pleiades	0,869	1,377	0,768	1,073	1,756	74,503	59,883	76,959	77,661
Quickbird	0,842	1,317	0,738	1,061	1,721	73,372	58,023	73,488	75,930
Formosat-2	0,849	1,353	0,651	1,059	1,744	73,216	59,649	74,269	76,491
Landsat	0,926	1,421	1,170	1,138	1,765	76,140	75,439	76,257	79,532
Spot 5-HRV	0,866	1,324	0,909	1,096	1,718	72,749	73,567	75,322	77,544
Meris	1,216	1,974	1,862	1,237	1,999	76,118	61,882	78,471	79,529

Table 6. NCGIA

Sensor	JM_{wave}	JM_{ave}	JM_{min}	TD_{wave}	TD_{ave}	1NN	NaiveBayes	J48	Vote
Ikonos	1,386	1,946	1,497	1,409	1,977	57,895	42,857	57,895	59,398
Pleiades	1,386	1,940	1,474	1,162	1,824	57,143	44,361	56,391	62,406
Quickbird	1,393	1,952	1,578	1,410	1,976	59,398	42,857	54,887	61,654
Formosat	1,382	1,942	1,444	1,338	1,939	56,391	42,857	54,887	60,150
Landsat	1,419	1,977	1,705	1,449	1,998	57,143	59,398	57,895	60,902
Spot 5-HRV	1,371	1,939	1,380	1,405	1,970	55,639	44,361	59,398	63,158
Meris	0,766	1,441	0,135	1,438	1,984	53,030	36,364	58,333	56,818

Table 7. USGS

Sensor	Level	JM_{wave}	JM_{ave}	JM_{min}	TD_{wave}	TD_{ave}	1NN	NaiveBayes	J48	Vote
Ikonos	I	0,790	1,920	1,819	0,827	1,994	97,490	64,958	94,456	96,444
-	II	1,284	1,966	1,512	1,327	1,985	93,410	56,590	87,866	91,527
-	III	1,763	1,949	1,067	1,769	1,954	87,552	59,414	80,544	85,669
-	IV	1,840	1,956	1,402	1,838	1,953	87,552	57,322	81,276	85,356
Pleiades	I	0,787	1,903	1,810	0,808	1,956	98,222	61,402	96,339	96,548
-	II	1,263	1,946	1,464	1,024	1,920	93,933	56,276	87,029	91,841
-	III	1,741	1,929	1,139	1,608	1,821	89,644	60,669	82,113	86,611
-	IV	1,810	1,924	1,238	1,695	1,771	89,121	59,937	81,590	86,715
Quickbird	I	0,782	1,913	1,794	0,827	1,994	98,013	65,377	95,188	96,444
-	II	1,301	1,966	1,573	1,322	1,985	93,305	56,276	86,715	90,586
-	III	1,764	1,948	1,109	1,771	1,954	87,866	59,728	79,916	85,146
-	IV	1,840	1,958	1,350	1,839	1,954	87,552	58,264	80,962	85,251
Formosat-2	I	0,782	1,897	1,784	0,825	1,989	98,222	64,226	95,607	96,862
-	II	1,232	1,947	1,345	1,177	1,962	94,038	56,695	86,088	91,736
-	III	1,750	1,938	1,110	1,713	1,911	88,285	59,937	79,498	85,356
-	IV	1,828	1,946	1,304	1,796	1,902	87,866	58,473	80,858	85,146
Landsat	I	0,814	1,967	1,923	0,830	2,000	99,582	79,707	96,234	97,803
-	II	1,314	1,981	1,595	1,374	1,993	96,548	53,556	88,598	93,305
-	III	1,809	1,976	1,469	1,821	1,980	93,619	65,272	85,669	91,423
-	IV	1,856	1,963	0,546	1,859	1,976	92,887	69,979	87,762	90,690
Spot 5-HRV	I	0,789	1,907	1,784	0,830	2,000	98,745	79,707	96,025	96,757
-	II	1,291	1,964	1,549	1,317	1,985	94,979	57,008	86,402	91,632
-	III	1,782	1,956	1,153	1,803	1,967	91,423	63,075	82,531	88,180
-	IV	1,841	1,961	0,950	1,849	1,960	90,377	65,481	82,741	88,389
Meris	I	0,756	1,719	1,163	0,830	1,999	98,222	65,481	97,280	97,280
-	II	0,896	1,839	0,179	1,347	1,989	94,142	54,289	87,657	92,259
-	III	1,553	1,802	0,346	1,711	1,927	89,749	58,473	83,787	88,389
-	IV	1,754	1,846	0,246	1,813	1,925	89,121	59,728	83,264	87,448

Table 8. Evaluation of the influence of the NDVI channel on the different sensors.

	Aster 1	Aster 2	Aster 3	NCGIA	USGS	Herold1	Herold 2	Herold 3	Herold 4
Ikonos	83,333	53,333	45,185	59,398	77,093	96,444	91,527	85,669	85,356
+ NDVI	83,704 ↗	54,444 ↗	45,556 ↗	60,902 ↗	76,860 ↘	97,490 ↗	92,364 ↗	88,912 ↗	87,866 ↗
Pleiades	92,222	61,111	50,000	62,406	77,661	96,548	91,841	86,611	86,715
+ NDVI	93,704 ↗	61,852 ↗	51,852 ↗	57,895 ↘	79,064 ↗	97,385 ↗	91,213 ↘	88,389 ↗	88,912 ↗
Quickbird	84,444	51,481	44,815	61,654	75,930	96,444	90,586	85,146	85,251
+ NDVI	84,074 ↘	55,926 ↗	45,185 ↗	60,150 ↘	76,744 ↗	97,803 ↗	91,527 ↗	87,971 ↗	88,598 ↗
Spot 5-HRV	89,259	57,778	50,741	63,158	77,544	96,757	91,632	88,180	88,389
+ NDVI	87,037 ↘	56,667 ↘	44,074 ↘	60,150 ↘	78,363 ↗	96,967 ↗	92,259 ↗	88,285 ↗	88,598 ↗

Table 9. Evaluation of the influence of the SWIR channel on the Spot 5-HRV and Pleiades sensors.

	Aster 1	Aster 2	Aster 3	NCGIA	USGS	Herold1	Herold 2	Herold 3	Herold 4
Pleiades	92,222	61,111	50,000	62,406	77,661	96,548	91,841	86,611	86,715
+ MIR	88,889 ↘	62,963 ↗	49,630 ↘	62,406 →	78,246 ↗	96,967 ↗	92,992 ↗	88,598 ↗	89,121 ↗
Spot 5-HRV	89,259	57,778	50,741	63,158	77,544	96,757	91,632	88,180	88,389
- MIR	87,778 ↘	55,556 ↘	48,889 ↘	57,143 ↘	75,322 ↘	95,816 ↘	90,795 ↘	83,054 ↘	84,623 ↘